Lossless Compression of Medical Images Using 3-D Predictors

*Luís F. R. Lucas, Nuno M. M. Rodrigues, Luis A. da Silva Cruz, and Sérgio M. M. de Faria

Abstract—This paper describes a highly efficient method for lossless compression of volumetric sets of medical images, such as CTs or MRIs. The proposed method, referred to as 3-D-MRP, is based on the principle of minimum rate predictors (MRPs), which is one of the state-of-the-art lossless compression technologies presented in the data compression literature. The main features of the proposed method include the use of 3-D predictors, 3-D-block octree partitioning and classification, volume-based optimization, and support for 16-b-depth images. Experimental results demonstrate the efficiency of the 3-D-MRP algorithm for the compression of volumetric sets of medical images, achieving gains above 15% and 12% for 8- and 16-bit-depth contents, respectively, when compared with JPEG-LS, JPEG2000, CALIC, and HEVC, as well as other proposals based on the MRP algorithm.

Index Terms—Minimum rate predictors, 3D predictors, lossless compression, medical image compression, volumetric data compression.

I. Introduction

THE use of medical imaging systems for diagnosis purposes is a standard in current healthcare practices. With the advance of scanning technologies and digital systems in the last decades, these systems have become increasingly important, producing more accurate images with improved quality, using higher spatial resolutions and bit depths. Such improvements increase the amount of information that needs to be processed, transmitted and stored. This is particularly relevant when using volumetric scanning technologies, such as Computed Tomography (CT) or Magnetic Resonance Imaging (MRI), which produce multiple image slices.

These facts, associated to the increasing number of archiving databases of medical images deployed by healthcare providers, motivate the research of efficient compression methods for these signals. For this purpose, it is important to use lossless compression algorithms to avoid introducing errors in the data outputted by the scanning system.

In this context, this paper investigates a native 3D coding solution based on minimum rate predictors (3D-MRP) targeted at lossless compression of volumetric medical images. In the proposed algorithm, the input data is processed at volume-level, using not only 3D predictors, but also 3D block classification, volume-based optimisation, 3D context modelling, among other improvements. As the use of high bit-depth images is a common practice in medical imaging systems, the 3D-MRP algorithm was designed to handle images with pixel bit-depths up to 16 bits. Experimental results show that the proposed 3D-MRP algorithm is able to achieve higher performance than existing state-of-the-art approaches for lossless compression of volumetric sets of medical data.

This paper is organized as follows. Section II reviews the main existing algorithms that can be used for lossless compression of medical images. Section III describes the original MRP algorithm for image compression, which is the core of the proposed method. In Section IV, the 3D-MRP proposed for the compression of volumetric sets of medical images is described. Section V presents and discusses the experimental results. Finally, Section VI concludes the paper.

II. Algorithms for Lossless Compression of Medical Images

Most medical imaging systems adopt the recommendations of the Digital Imaging and Communications in Medicine (DICOM) organization [1], which stipulates the use of several major image coding standards, including JPEG [2], [3], Lossless JPEG (JPEG-LS) [4], [5], JPEG2000 [6], [7], Run Length Encoding (RLE), as well as video coding standards, such as MPEG2 [8] and H.264/AVC [9], [10].

JPEG and JPEG2000 are transform-based standards, which use Discrete Cosine Transform (DCT) and Discrete Wavelet Transform (DWT), respectively. The latter presents a superior compression performance and supports a set of desirable features, such as region-of-interest (ROI) coding, lossy-to-lossless coding, resolution scalability and resilience against transmission errors. The superiority of JPEG2000 is also justified by

its volumetric extensions, which provide extra functionality for the compression of volumetric data, such as the Multi Component Transform (MCT) feature (Part 2 of JPEG2000) [11] and a 3D extension, JP3D (Part 10 of JPEG2000) [12]. While the first solution interprets the multiple image slices as separate image components, the JP3D part extends the core techniques of JPEG2000 to encode the input data as a volume, namely by expanding DWT to three dimensions (3D-DWT).

The JPEG-LS standard uses the LOw COmplexity LOssless COmpression for Images (LOCO-I) algorithm, which is based on predictive coding. Its main limitation is the inability to exploit inter-slice redundancies, which makes it inefficient for the compression of volumetric data. An efficient alternative to encode this data is to use video coding standards, namely the MPEG2 and H.264/AVC, as well as the most recent state-of-the-art High Efficiency Video Coding (HEVC) [13], [14] standard.

In addition to the existing video coding standards, alternative compression methods have been proposed in the literature for application to medical image compression. Most of these methods improve the existing standards for the compression of medical images, either by proposing new techniques [15]–[17], or by removing unimportant image regions not required for medical diagnosis (e.g. the background regions) [18]. A class of lossless compression algorithms, which tends to be more efficient than the existing transform-based standards, is based only on predictive coding (no transformations are employed). The main drawback of prediction-based algorithms is the high computational complexity and the absence of some coding features, such as resolution scalability or ROI coding.

Some of the most important compression algorithms in this class include the Context Based Adaptive Lossless Image Codec (CALIC) [19], the Edge-Directed Prediction (EDP) [20] and the Minimum Rate Predictors (MRP) [21], [22]. While most of these methods were developed for still image coding, some of them have been also extended for lossless compression of video or volumetric data. Some examples are the M-CALIC [23], 3D-CALIC algorithm [24] and several 3D extensions of MRP for lossless video compression.

Existing MRP-based solutions for video compression use up to two causal frames to form a 3D linear predictor able to exploit inter-frame similarities [25]–[27]. As these methods are designed for generic video signals, they first apply motion compensation methods, and then optimise the predictor defined in the current and previous compressed frames. While the proposal of [26] employs non-sequential compression of video frames in order to use bi-prediction based on both past and future temporal frames, the work of [27] is able to achieve a superior compression performance by exploiting only past temporal frames, which are adaptively selected. In [28], MRP is investigated for the compression of volumetric medical images by processing each frame sequentially and using 3D predictors based on the previously encoded frames.

III. THE MINIMUM RATE PREDICTORS ALGORITHM

The Minimum Rate Predictors (MRP) algorithm was originally proposed for lossless compression of still images. It is
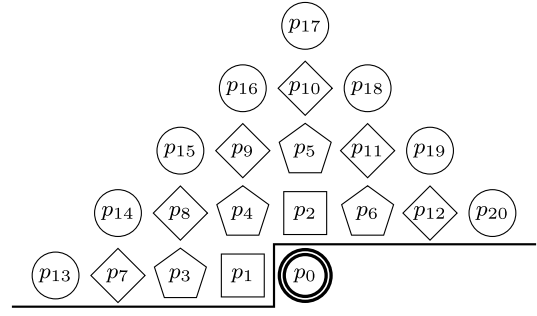

Fig. 1. Example of a prediction support in MRP algorithm for $K = 20$.

one of the most efficient methods presented in the literature, being the core technology of the 3D-MRP method proposed in this paper.

MRP uses an asymmetric coding procedure which concentrates most of the computational burden at the encoder side, enabling a practical decoder algorithm with low complexity. The last available version of the MRP software [29] for the compression of grayscale images is described in this section. A complete description of this software is not available in literature, although the two main optimisation loops of MRP algorithm are independently described in [21] and [22].

A. General Overview

The underlying principle of MRP is to perform linear prediction using a set of coefficients optimally designed to minimize the residue bitrate. It differs from most prediction-based algorithms, such as EDP [20], which estimate the linear predictors by minimizing the residue energy. Furthermore, it uses a forward design of the predictors, where the linear coefficients are quantised and transmitted to the decoder side.

MRP employs an adaptive block-based prediction technique, classifying each image block into one of M classes associated to different predictors. Each predictor is based on the K previous encoded reference pixels, ordered by an increasing Manhattan distance from the unknown pixel ($\mathbf{p}_0$), as illustrated in Figure 1 (for $K = 20$).

The prediction of pixel $\mathbf{p}_0$, belonging to a block assigned to the m-th class (with $m = 1, 2, \ldots, M$) is given by:

$$\hat{s}(\mathbf{p}_0) = \sum_{k=1}^{K} a_m(k) \cdot s(\mathbf{p}_k) \qquad (1)$$

where $a_m(k)$ (with $k = 1, 2, \ldots, K$) is the linear coefficient associated with the reference pixel $\mathbf{p}_k$, and $s(\mathbf{p}_k)$ is the brightness value of pixel $\mathbf{p}_k$. After the prediction, the residue signal given by $e = s(\mathbf{p}_0) - \hat{s}(\mathbf{p}_0)$, is entropy coded using context modelling and arithmetic coding.

The context modelling infers the probability density function (PDF) of the error, based on the previous encoded error values in the causal neighbourhood. This process involves computing a characteristic quantity U using

$$U = \sum_{k=1}^{12} \frac{1}{\delta_k} \cdot E_k \qquad (2)$$

where E_k is an error index [21], which corresponds to a non-negative mapping of the error e at the position of the reference pixel $\mathbf{p}_k$, and δ_k is a weighting factor equal to the Euclidean distance between the reference pixel $\mathbf{p}_k$ and the pixel to be predicted $\mathbf{p}_0$.

The U quantity is an estimation of the prediction error PDF. To encode the error, MRP uses one out of 16 PDFs, selected based on a non-linear quantisation of U into 16 levels (or groups). This quantisation is performed based on 15 threshold values $Th_m(1), Th_m(2), \ldots, Th_m(15)$ optimised during the encoding process and explicitly signalled in the bitstream.

For coding optimisation, MRP repeatedly alternates between three functions: design of the minimum rate predictors, estimation of quantisation thresholds and classification of the blocks, so that the global coding cost is minimized. The last available implementation of MRP [29] uses two optimisation stages, which are described in the following sub-sections.

B. First Optimisation Stage

MRP starts by dividing the input image into blocks of 8×8 pixels and computing the luminance variance of each block, which is used for the initial block classification. The design of the predictors is the first step of the iterative optimisation. MRP assumes that the prediction errors e are modelled by a Gaussian PDF, given by:

$$P(e) = \frac{1}{\sqrt{2\pi\sigma^2}} \cdot \exp\left(-\frac{e^2}{2\sigma^2}\right). \tag{3}$$

Assuming that e is quantised using a sufficiently small step-size, Δe, the number of bits used to represent the quantised error, $\hat{e}$, can be approximated by $L(\hat{e}) = -\log_2\left(P(e) \cdot \Delta e\right)$. For a set of pixels classified within the same class, $\mathbf{C}$, the total residue bitrate for that class, $R(\mathbf{C})$, is given by:

$$R(\mathbf{C}) = \sum_{\mathbf{p}_0 \in \mathbf{C}} L(\hat{e}) = -\sum_{\mathbf{p}_0 \in \mathbf{C}} \log_2\left(P(e) \cdot \Delta e\right)$$
$$= -\sum_{\mathbf{p}_0 \in \mathbf{C}} \log_2\left(\frac{\Delta e}{\sqrt{2\pi\sigma^2}}\right) + \frac{\log_2 \epsilon}{2} \cdot \sum_{\mathbf{p}_0 \in \mathbf{C}} \frac{e^2}{\sigma^2}, \tag{4}$$

where ϵ is the Euler's constant.

The minimum rate predictors for the set of pixels $\mathbf{C}$ are found by minimizing Equation 4, resulting in a weighted least-squares (WLS) problem for each class, where the weights are given by the inverse of the prediction error variance σ^2. This variance is estimated from the U quantity, that is quantised into 16 levels (or groups/contexts). The quantized variance values were defined in such a way that the entropy (H_n) of the errors at each group/context is an arithmetic progression ranging from $H_1 = 0.1$ up to $H_{16} = 7.0$ bits [30].

After the predictors, MRP optimises the threshold values used for non-linear quantisation of the U quantity. The group into which the U is quantised defines the variance of the Gaussian PDF used for error modelling. MRP determines the optimal threshold values through the use of dynamic programming methods that minimize the errors coding cost for each class [22]. Using the updated predictors and thresholds, MRP reclassifies all the 8×8 blocks by testing all the available classes, and selecting the ones that minimize the residue

coding cost. The estimation procedure for the predictors and thresholds is repeated while the total residue coding cost decreases, until a maximum of 100 iterations, or when the coding cost stops decreasing during 10 consecutive iterations.

C. Second Optimisation Stage

The linear predictors, thresholds and block classification obtained in the first optimisation stage are not encoded but used as starting point for the second stage. In this stage, the prediction errors in each context are modelled by generalized Gaussian PDFs, which tend to provide more accurate prediction error models for some images, namely when the actual distribution of the prediction errors presents sharp peaks [22].

The probability of the error can be obtained by integrating the generalized Gaussian PDFs over a region, as follows:

$$\Pr(e|n) = \int_{-h_s/2}^{h_s/2} \tilde{P}(e + \varepsilon|n) \, d\varepsilon \tag{5}$$

where h_s is the quantisation step for the error and $\tilde{P}(e|n)$ is the generalized Gaussian PDF of the error for context/group n, which is given by:

$$\tilde{P}(e|n) = \frac{c_n \cdot \eta(c_n, \sigma_n)}{2\Gamma(1/c_n)} \cdot \exp\left\{-|\eta(c_n, \sigma_n) \cdot e|^{c_n}\right\},$$
$$\eta(c_n, \sigma_n) = \frac{1}{\sigma_n}\sqrt{\frac{\Gamma(3/c_n)}{\Gamma(1/c_n)}}, \tag{6}$$

where $\Gamma(\cdot)$ is the Gamma function, σ_n is the standard deviation and c_n is the shape parameter of the generalized Gaussian. The values of σ_n are fixed for each group n, being the same as the ones used in the first stage for error modelling using Gaussian PDFs. The c_n value is adaptively determined for each group.

Given that the input images use 8 bit-depth representation and the predicted value $\hat{s}(\mathbf{p}_0)$ is always known, the prediction error e can be restricted to 256 values, as follows:

$$e \in \{s - \hat{s}(\mathbf{p}_0) \mid s = 0, 1, \ldots, 255\}. \tag{7}$$

Thus, the conditional probability of the prediction error e, given the prediction $\hat{s}(\mathbf{p}_0)$, and context n (obtained by quantising U), can be computed based on Equation 5, as follows:

$$\Pr(e|\hat{s}(\mathbf{p}_0), n) = \frac{\Pr(e|n)}{\sum_{s=0}^{255} \Pr(s - \hat{s}(\mathbf{p}_0)|n)}. \tag{8}$$

Equation 8 is used for arithmetic coding of the prediction errors, as well as for estimation of the coding costs, using:

$$L(e|\hat{s}(\mathbf{p}_0), n) = -\log_2 \Pr(e|\hat{s}(\mathbf{p}_0), n)$$
$$= \log_2\left\{\sum_{s=0}^{255} \Pr(s - \hat{s}(\mathbf{p}_0)|n)\right\} - \log_2 \Pr(e|n). \tag{9}$$

The first step of this stage is to optimise the linear predictors. Due to the new model, the analytical solution based on WLS cannot be used to obtain the minimum rate solution for Equation 9. Thus, MRP simply refines the existing predictors by applying small corrections to the linear coefficients [22].

For coding cost estimation, a quantisation step $h_s = 1/8$ is used (see Equation 5).

For the coding cost estimation, MRP considers not only the cost of the prediction errors, but also the bitrate associated to the side information, which results in:

$$J = \sum_{\mathbf{p}_0} L(e|\hat{s}(\mathbf{p}_0), n) + B_a + B_t + B_m \qquad (10)$$

where the first term is the error bitrate (defined in Equation 9), and the remaining terms correspond to the side information used for transmission of the prediction coefficients, thresholds and block classification, respectively [22].

The threshold values are optimised as described in the first optimisation stage. The c_n parameter associated to the shape of the generalized Gaussian functions (see Equation 6) is also optimised by testing 16 values, specifically $c_n = 0.2, 0.4, \ldots, 3.2$. The last step is to reclassify the image blocks considering the updated linear predictors and thresholds. In contrast to the first stage, MRP employs an adaptive quadtree block partitioning scheme in this stage, with block sizes varying from 32×32 to 2×2 pixels.

These optimisation functions are iteratively processed until the global coding cost, based on Equation 10, stops decreasing during 10 consecutive iterations, or for a maximum of 100 iterations. Finally, the obtained prediction errors, linear coefficients, thresholds, shape parameters and block classification are entropy encoded using the range coder implementation of the arithmetic coding.

IV. PROPOSED VOLUMETRIC MRP

In this section the proposed 3D-MRP algorithm for lossless compression of volumetric medical images is presented. At its core, the 3D-MRP algorithm uses the MRP technology, as presented in the previous section. Thus, only the main contributions and differences relative to the existing MRP algorithm are described here.

A. 3D-Shaped Predictors

Besides the spatial redundancy, video (and volumetric) signals present inter-frame redundancy, which refers to the similarities between different frames of the signal. In order to exploit these dependencies, the previously presented MRP-based algorithms incorporate 3D predictors. Such predictors are able to estimate the unknown samples based not only on the spatial causal neighbouring samples, but also on samples from previously encoded frames.

In this work, a similar approach is adopted to exploit the spatial and inter-frame dependencies in the volumetric signals. Since this work is focused on volumetric medical images, it is assumed that the human body structures represented by these volumes have similar redundancy, either in horizontal, vertical or axial directions. While this assumption may not be precise for some signals, namely when they present a significant lower resolution along the axial direction, it seems a reasonable assumption for the majority of volumetric medical images, specially when they are captured by recent scanning systems, which tend to use higher resolutions along the axial direction.

Figure 2/ represents the proposed prediction support, which is based on 64 causal pixels. The reference pixels are selected in order of increasing Manhattan distance from the current predicting pixel ($\mathbf{p}_0$), assuming unitary distance between two neighbouring pixels in the horizontal, vertical and axial directions. Pixels located at different frames are independently represented in Figure 2 with the Z coordinate indicating their distance relative to the current frame ($Z = 0$) in the axial direction. Note that, since each pixel of the volumetric data is sequentially processed, from left to right, top to bottom, and from the first to last frame, the proposed predictor does not include pixels from future frames, and only causal pixels of the current frame can be included.

In the proposed predictor, based on 64 reference pixels, the most distant pixel used for prediction is at a distance of 4 pixels in the horizontal, vertical or axial directions. This means that 4 causal frames can be used by the proposed predictor, which contrasts to the existing MRP-based video coding solutions, whose predictors may use up to two reference frames.

B. Volume-Based Optimisation

While the use of 3D predictors is an important adaptation for the compression of volumetric data, the existing MRP-based algorithms still use a 2D data processing approach, operating in a frame-by-frame basis. This implies splitting the input volumetric data 2D images, and independently optimising and encoding the predictors, classes and thresholds for each image.

An alternative approach, used in 3D-MRP, is the design and optimisation of the linear predictors at the volume-level. By optimising a whole volume (*i.e.* a set of frames) instead of individual frames, the same predictors can be reused for a larger amount of pixels. This behaviour is advantageous to reduce the amount of side information that MRP uses for transmission of the predictors and thresholds. For instance, when a specific texture region is present along a set of frames, the optimal predictor for such texture area does not need to be repeatedly designed and signalled for each frame, as for the existing frame-based proposals of MRP algorithm.

To maximize the compression performance, 3D-MRP divides the input volumetric signal into fixed sized sub-volumes, which are sequentially processed and independently optimised. Using sub-volumes is advantageous when the amount of frames of the input data is quite large. This is because the statistics of the signal tend to vary along the axial direction, and thus the classes do not need to be reused along the entire volume. Based on several experiments, the chosen value for the sub-volume size along the axial direction was set to 32 frames. The width and height of the sub-volume are the same as the resolution of the volumetric medical image.

C. Hybrid 3D-Block Classification

As explained in Section III, the MRP algorithm classifies each block of the image into some class and predicts its pixels using the predictor associated with the selected class.
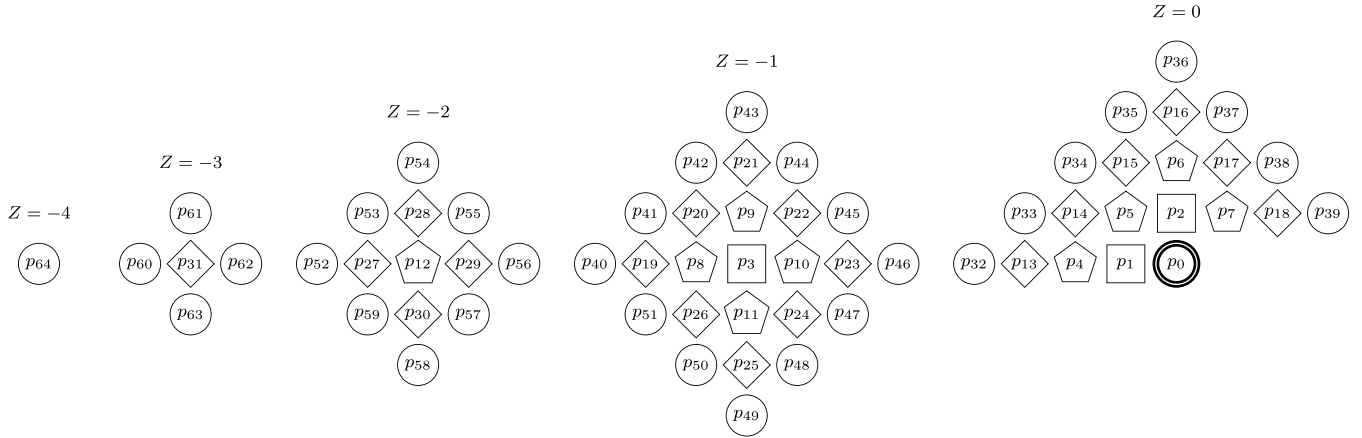
Fig. 2.   3D-shaped support used for linear prediction in the proposed 3D-MRP algorithm. Pixels located at previous frames are indexed by the Z coordinate, with $Z = 0$ corresponding to the current frame.
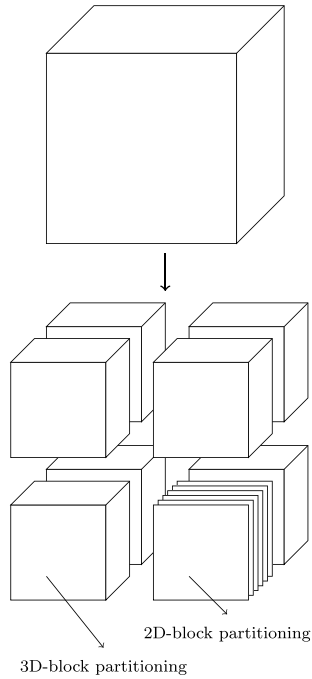

Fig. 3.   Octree-based partitioning of a 3D-block, with one of the sub-blocks (in the bottom-right corner) being further divided into independent 2D-blocks, as proposed by the hybrid classification step of 3D-MRP algorithm.

A similar procedure is performed for each frame encoded by the existing video-based extensions of MRP algorithm. While 3D-MRP may classify the medical image volume at block level, an alternative method based on 3D-blocks, *i.e.* cubes of pixels, was investigated.

The proposed 3D-classification approach was motivated by the fact that the same class can be assigned to multiple neighbouring blocks in consecutive frames. This avoids to repeat the signalling of the same class for the neighbouring blocks. In addition to 3D-blocks, the proposed classification method may also use 2D-blocks, specially for those regions where the 3D-blocks do not present any benefit. This feature results in a hybrid 3D/2D classification method.

The use of 3D-blocks in the proposed method motivated the research of an appropriate block partitioning scheme able to provide block sizes from $32 \times 32 \times 32$ down to $2 \times 2 \times 2$ pixels. In this context, an octree-based partitioning scheme is proposed, as illustrated in Figure 3, where each 3D-block is partitioned into 8 equally-sized 3D-sub-blocks. The octree partitioning is signalled similarly to the quadtree one, by transmitting one binary flag for each node of the partitioning tree, indicating whether the partitioning occurs or not.

For 2D-block classification, it is proposed a straightforward solution which divides the 3D-block into a set of 2D-blocks, one for each frame, as represented in the bottom-right corner of Figure 3. During the classification procedure, 3D-MRP evaluates the cost of each 3D-block, considering two classification possibilities, namely using a single class for all the pixels of the 3D-block, or using multiple classes, one per 2D-block that slices the 3D-block perpendicularly to the axial direction. For bitstream signalling, an additional binary flag is used to indicate whether the 3D-block is partitioned into 2D-blocks or not. This additional flag only needs to be transmitted when the 3D-block is not further partitioned by the octree scheme.

D. General Improvements

As described in previous sub-sections, 3D-MRP presents several improvements relative to the original MRP algorithm, designed for still image compression. Considering the new features of 3D-MRP algorithm, the values of some default MRP parameters were reviewed. In particular the number of classes available for each sub-volume, the number of groups (or contexts) used for prediction error modelling, and the calculation of the U quantity, originally given by Equation 2.

The original MRP algorithm automatically sets the number of available classes for the image based on

$$M = \lfloor 10.4 \cdot 10^{-5} X + 13.8 \rfloor , \tag{11}$$

where X is the number of pixels in the image. In 3D-MRP, it is required to define the number of classes used for each

sub-volume. Although the sub-volumes were configured with 32 frames, the number of frames of the last encoded sub-volume of the medical image volume may be smaller, depending on the number of remaining frames. Thus, it is proposed to automatically determine the number of available classes for each sub-volume, based not only on the image size but also on the number of frames present in the sub-volume. Based on several experiments it was found that a good estimate for the number of classes for the sub-volume is given by

$$T = \lfloor M + M \cdot 1/5 \cdot F_V \rfloor \qquad (12)$$

where M is given by Equation 11 and F_V is the number of frames in the sub-volume.

In this work, the number of groups used for prediction error modelling was also adjusted. Unlike the existing video-based extensions of MRP, which transmit the thresholds for non-linear quantisation of the U quantity at frame-level, the 3D-MRP algorithm only requires the signalling of this information for each sub-volume, *i.e.* every 32 frames. Considering that this behaviour results in a reduced overhead for the transmission of the thresholds, the use of an increased number of groups was investigated. From some experiments, the optimal number of groups was found to be 32, instead of 16 groups as in the original MRP. Due to the larger amount of groups, the standard deviation parameter associated with the probability distribution of each group was redefined. The standard deviation parameters were redesigned as discussed in Sub-section III-B, assuming 32 groups.

Another optimisation introduced in the design of the 3D-MRP algorithm was related to the computation of the U quantity. It is proposed to use not only pixels from the current frame, but also pixels from the previous frames. In practice, the U quantity in 3D-MRP algorithm is based on Equation 2, but it uses 31 causal pixels instead of 12. The main difference is related to the position of the error indexes E_k, which considers the neighbouring pixels from the current and previous frames, ordered by increasing Manhattan distance (see the first 31 pixels of Figure 2) from the current pixel. In order to compute the δ_k parameter of Equation 2, it is assumed that the distance between neighbouring pixels in the axial direction is the same as in the horizontal and vertical directions, being equal to 1.

E. Extension of MRP to 16 Bit-Depth Images

While the original MRP algorithm was designed for 8 bit-depth images, most medical images present higher bit depths, which can go up to 16 bits. This issue was addressed by properly designing the 3D-MRP algorithm to deal with higher bit-depth images. The major changes relative to the original MRP algorithm involved the redesign of the probability functions for prediction error modelling and the calculation of the U quantity.

The error probability function, $\Pr(e|\hat{s}(\mathbf{p}_0), n)$, given by Equation 8, was modified to consider the actual maximum pixel value of the input medical image, instead of the 255 value used for the 8 bit-depth images. In 3D-MRP, the maximum pixel value of the input medical image volume is determined

TABLE I
USED VALUES FOR F_i FUNCTION PARAMETERS a_i, b_i AND c_i

Function	max. pixel value	a_i	b_i	c_i
F_1	2^9 to $2^{10} - 1$	406.77	406.27	−2443.47
F_2	2^{10} to $2^{11} - 1$	218.79	218.29	−1178.36
F_3	2^{11} to $2^{12} - 1$	154.25	153.75	−776.70
F_4	2^{12} to $2^{13} - 1$	120.91	120.41	−579.26
F_5	2^{13} to $2^{14} - 1$	100.23	99.73	−461.30
F_6	2^{14} to $2^{15} - 1$	86.03	85.53	−382.73
F_7	2^{15} to $2^{16} - 1$	75.59	75.09	−326.45

before the compression procedure and transmitted to the decoder.

For efficient compression of the 16 bit-depth images, 3D-MRP also redesigned the standard deviation parameters of the error probability functions defined for each available group. For designing these parameters, a procedure similar to the one explained in Sub-section III-B was used. Thus, the standard deviation parameters were determined in such a way that the entropy (H_n) of the errors modelled by the Gaussian functions at each context is an arithmetic progression ranging from $H_1 = 0.1$ up to $H_N = B - 1$ bits, with N being the total number of groups in 3D-MRP, *i.e.* 32, and B being the minimum bit-depth required to represent the maximum pixel value in the volumetric medical image.

In regard to the calculation of the U quantity, an improved method suited for high bit-depth images was developed. It was observed that the original MRP algorithm limited the maximum value of the U quantity to 512. However, when compressing high bit-depth images, the residue values may be much larger, resulting in U quantity values significantly higher than 512. A possible improvement could be to increase the maximum value of the U quantity, but this solution would have an extremely high impact in the computational complexity. Thus, an alternative solution was proposed, by mapping the computed high bit-depth U quantity, referred to as U_h, to a reduced range U quantity, from 0 to 512, using a logarithmic function. The idea of the logarithmic mapping is to better preserve the smaller values of the U_h quantity, and quantise the larger values of U_h into fewer levels.

D-MRP algorithm defines 7 possible mapping functions, which depend on the maximum value present in the medical image volume. When the maximum value of the image is inferior to 512 (or 2^9) the mapping feature is not used. These mapping functions, $U = F_i (U_h)$, with $i = 1, \ldots, 7$, are given by:

$$U = F_i(U_h) = \text{round}(a_i \cdot \log(b_i + U_h) + c_i) \qquad (13)$$

where log corresponds to the natural logarithm and U_h is computed as explained in Sub-section IV-D, based on Equation 2, using 31 causal pixels.

Table I specifies the parameters, a_i, b_i and c_i of the proposed logarithmic mapping functions F_i, as well as the range of maximum pixel value used to select the mapping function. These function parameters were derived so that the following conditions were satisfied (ignoring the round function of F_i):

1) $F_i (0) = 0 \quad \Leftrightarrow \quad a_i \cdot \log(b_i + 0) + c_i = 0$
2) $F_i (1) = 1 \quad \Leftrightarrow \quad a_i \cdot \log(b_i + 1) + c_i = 1$
3) $F_i (U_{M_i}) = 512 \quad \Leftrightarrow \quad a_i \cdot \log(b_i + U_{M_i}) + c_i = 512$

TABLE II
TEST SET 1 COMPOSED OF 8 BIT-DEPTH MEDICAL IMAGES

Sequence	Resolution	Frames
CT_Aperts	256×256	97
CT_Carotid	256×256	74
CT_Skull	256×256	203
CT_Wrist	256×256	183
MR_Liver_T1	256×256	58
MR_Liver_T2e1	256×256	58
MR_Ped_Chest	256×256	77
MR_Sag_Head	256×256	58

TABLE III
TEST SET 2 COMPOSED OF 16 BIT-DEPTH MEDICAL IMAGES

Sequence	Resolution	Frames	Max. value
CT_Head	256×256	99	3272
CT_Head_Remb [35]	256×256	58	1377
CT_Lung_R4 [36], [37]	512×512	68	4096
CT_Lung_R13 [36], [37]	512×512	67	4095
CT_Esophagus [38]	512×512	166	4094
MR_Brain	256×256	99	5119
MR_Neuro [39]	256×256	176	1328
MR_Breast [40]	288×288	60	13849

TABLE IV
COMPRESSION RESULTS (IN BPP) OF 3D-MRP ALGORITHM FOR A
VARYING NUMBER OF GROUPS

No. groups:	16	20	24	28	32	36
Avg. Test Set 1:	0.893	0.890	0.888	0.886	**0.886**	0.886
Avg. Test Set 2:	4.396	4.391	4.387	4.385	**4.384**	4.384

TABLE V
COMPRESSION RESULTS (IN BPP) OF 3D-MRP ALGORITHM FOR A
VARYING NUMBER OF CLASSES

Constant of Eq. 12:	1/3	1/4	1/5	1/6
Avg. Test Set 1:	0.887	0.887	**0.886**	0.889
Avg. Test Set 2:	4.385	4.384	**4.384**	4.384

TABLE VI
COMPRESSION RESULTS (IN BPP) OF 3D-MRP ALGORITHM FOR
VARYING PREDICTION ORDER

Prediction order:	12	31	64	115
Avg. Test Set 1:	1.043	0.916	**0.886**	0.898
Avg. Test Set 2:	4.502	4.417	4.384	**4.377**

TABLE VII
COMPRESSION RESULTS (IN BPP) OF 3D-MRP ALGORITHM USING
DIFFERENT CLASSIFICATION METHODS

Classification method:	2D	3D	2D&3D
Avg. Test Set 1:	**0.885**	1.020	0.886
Avg. Test Set 2:	4.402	4.394	**4.384**

where U_{M_i} is the maximum value of U_h quantity considered for each mapping function F_i, which was defined as $U_{M_i} = 2 \cdot 2^{i+8}$. This expression assumes that the maximum value of U_h quantity for some image is at most twice the maximum pixel value, defined in Table I for each function F_i.

V. EXPERIMENTAL RESULTS

Several experiments were performed using the 3D-MRP algorithm, comparing it with existing methods for the compression of volumetric sets of medical images. Two versions of 3D-MRP using a maximum of 3 and 25 iterations for each optimisation stage were tested. For the compression of volumetric medical images, 3D-MRP processes the first frame as an independent sub-volume (since it only uses spatial predictors), while the remaining frames are encoded using the default sub-volume size with 32 frames. For all the performed tests, the compression performance results are presented in bits-per-pixel (bpp).

Two main data sets of medical images were considered in the experimental tests. The Test Set 1 [31], presented in Table II, only contains 8 bit-depth images. The Test Set 2, presented in Table III, includes medical images from two sources, which present larger bit-depths (16 bits per pixel in the uncompressed format). The CT_Head and MR_Brain belong to the Stanford volume data archive [32], while the remaining medical images belong to the Cancer Imaging Archive [33], [34]. Table III also shows the maximum pixel value present in each medical image of the Test Set 2, which tends to be quite inferior than $2^{16} - 1$.

A. Parameter Evaluation in 3D-MRP Algorithm

In this sub-section, the influence of some parameters of 3D-MRP algorithm on its compression performance is analysed. The parameters evaluated are the number of classes for each

sub-volume, the number of groups and the prediction order. The importance of the hybrid classification method based on both 2D and 3D-blocks is also demonstrated. For each evaluated parameter, several experimental tests were performed by varying its value, while keeping the remaining settings fixed.

Table IV presents the average compression results of 3D-MRP (using up to 25 iterations) for a variable number of groups, with the prediction order being 64 and the number of classes of each sub-volume being given by Equation 12. Although the original MRP algorithm was designed to use 16 groups, the results of Table IV show that 3D-MRP algorithm is improved when using a larger number of groups. Since the compression gains are null when the number of groups is larger than 32, this value was selected as being the optimal one. By defining the number of groups equal to 32, average compression gains were 0.007 bpp for Test Set 1 and more than 0.01 bpp for Test Set 2.

Table V presents the average compression results when changing the constant value used to determine the number of classes of each sub-volume (defined in Equation 12 with 1/5 value by default). From these results, one observes that the compression performance does not have a significant variation when different numbers of classes are available. Thus, the value 1/5 was selected.

As previously explained, 3D-MRP uses a 3D-shaped predictor based on 64 causal pixels, whose positions present a maximum Manhattan distance of 4 relative to the unknown

TABLE VIII
COMPRESSION PERFORMANCE RESULTS (IN BPP) FOR TEST SET 1 USING 3D-MRP AND OTHER EXISTING COMPRESSION METHODS FOR 8 BIT-DEPTH CONTENTS

Test Set 1	JPEG-LS	JPEG2000	JP3D	CALIC	M-CALIC	3D-CALIC	HEVC-Rext	MRP-[29]	MRP-Video-[28]	3D-MRP-I3	3D-MRP-I25
CT_Aperts	1.058	1.261	0.941	0.998	1.205	0.994	0.728	0.775	0.533	0.465	**0.447**
CT_Carotid	1.778	2.019	1.547	1.684	1.800	1.517	1.425	1.374	1.043	0.891	**0.849**
CT_Skull	2.761	2.991	2.088	2.628	2.585	2.153	1.766	2.329	1.253	1.168	**1.097**
CT_Wrist	1.627	1.757	1.238	1.551	1.435	1.127	1.002	1.173	0.641	0.553	**0.524**
MR_Liver_T1	3.160	3.256	1.745	3.022	2.832	2.323	2.052	2.582	1.480	1.397	**1.332**
MR_Liver_T2e1	2.418	2.572	2.356	2.269	2.179	1.828	1.509	1.722	0.931	0.877	**0.814**
MR_Ped_Chest	2.937	3.021	2.071	2.789	2.213	1.860	1.534	2.337	1.099	0.935	**0.900**
MR_Sag_Head	2.582	2.905	2.160	2.519	2.605	2.329	1.748	2.279	1.367	1.169	**1.122**
Average	2.290	2.473	1.768	2.183	2.107	1.766	1.470	1.821	1.043	0.932	**0.886**

TABLE IX
COMPRESSION PERFORMANCE RESULTS (IN BPP) FOR TEST SET 2 USING 3D-MRP AND OTHER EXISTING COMPRESSION METHODS FOR 16 BIT-DEPTH CONTENTS

Test Set 2	JPEG-LS	JPEG2000	JP3D	2D-CALIC	M-CALIC	3D-CALIC	HEVC-Rext	3D-MRP-I3	3D-MRP-I25
CT_Head	4.996	5.185	4.915	4.847	5.210	4.960	4.745	4.160	**4.108**
CT_Head_Remb	5.486	5.397	5.420	5.208	5.678	5.512	5.400	4.722	**4.704**
CT_Lung_R4	5.800	6.011	5.968	5.812	5.969	5.896	5.743	5.281	**5.250**
CT_Lung_R13	5.655	5.536	5.623	5.437	6.098	5.729	5.837	4.792	**4.764**
CT_Esophagus	2.710	2.503	2.612	2.557	3.149	2.854	2.549	1.925	**1.909**
MR_Brain	6.651	6.934	7.007	6.625	6.902	6.842	6.530	6.253	**6.233**
MR_Neuro	5.295	5.367	5.162	5.119	5.383	5.341	5.066	4.625	**4.610**
MR_Breast	3.932	4.163	4.070	4.111	4.288	4.227	3.944	3.505	**3.495**
Average	5.066	5.137	5.097	4.965	5.337	5.170	4.977	4.408	**4.384**

pixel. In order to demonstrate the advantage of the proposed predictor, experiments were performed assuming different Manhattan distances, namely 2, 3, 4 and 5, which correspond to predictors based on 12, 31, 64 and 115 reference pixels, respectively. The average results obtained, given in Table VI, show that the 3D-shaped predictor based on 64 pixels provides the best compression results for the Test Set 1. The Test Set 2 presents a slight improvement when it uses the larger predictor. However, as this gain is small, $K = 64$ was used as the best compromise between compression efficiency and computational complexity.

The last set of experiments, presented in Table VII, evaluate the 2D, 3D and the hybrid classification methods for 3D-MRP algorithm. From the average results presented in Table VII, one observes that 2D classification tends to perform better than 3D classification. These results also show that the hybrid classification may be advantageous, in particular for the Test Set 2. In the case of Test Set 1, the compression performance of hybrid classification is quite similar to the one of 2D classification, presenting an insignificant bitrate increase. This can be justified by the slight overhead resulting from the additional signalling flag that indicates whether the 2D or 3D partitioning is used for each 3D-block. Nevertheless, despite this slight difference for Test Set 1, the overall compression results justify the adoption of the hybrid classification method in 3D-MRP.

B. Compression Performance for Volumetric Sets of Medical Images

In this sub-section, the 3D-MRP is compared with several methods for lossless compression of medical images. Table VIII presents the compression performance results

(in bpp) for each volumetric medical image of Test Set 1. Image-based codecs were used in the experiments by compressing independently each frame of the volumetric signal. The used image-based codecs include the HP implementation [41] of JPEG-LS [5], JPEG2000 (OpenJPEG software) [42], CALIC [43], and MRP version 0.5 [29]. Regarding the lossless codecs adapted for 3D contents or video signals, it was used the 3D extension of JPEG2000 (JP3D) [42], the M-CALIC and 3D-CALIC provided by Martin Briano [44], the HEVC (HM-16.9 reference software) [13] using the default random access configuration with main-RExt profile, and a video extension of MRP algorithm (MRP-Video), recently proposed in [28] for medical image coding.

From the compression results presented in Table VIII, one may observe the superiority of 3D-MRP method relative to the other methods, either using 3 (3D-MRP-I3) or 25 (3D-MRP-I25) iterations. The achieved compression gains of 3D-MRP-I25 over the recent MRP-based video codec [28] are superior to 0.15 bpp (or 15%). When the maximum number of iterations is reduced to 3 (3D-MRP-I3), the performance of 3D-MRP decreases about 5%, but it continues being more efficient than the other algorithms. As will be discussed in Sub-section V-C, the main advantage of 3D-MRP-I3 is its lower computational complexity.

As expected, the 3D and video-based encoders, which exploit inter-frame dependencies, tend to provide a superior compression performance. For instance, JP3D performs better than JPEG2000, and M-CALIC/3D-CALIC perform better than CALIC algorithm. Nevertheless, the best compression results are achieved by the algorithms based on the MRP paradigm, in particular the 3D-MRP and MRP-Video [28], providing gains larger than 0.4 bpp (30%) over the HEVC.

TABLE X

RUNNING TIMES (IN SECONDS) FOR THE COMPRESSION OF THE TEST SET 1 (8 BIT-DEPTH CONTENTS) USING JP3D, HEVC, MRP-VIDEO AND 3D-MRP

Test Set 1	JP3D		HEVC-Rext		MRP-Video [28]		3D-MRP-I3		3D-MRP-I25	
	Encoder	Decoder	Encoder	Decoder	Encoder	Decoder	Encoder	Decoder	Encoder	Decoder
CT_Aperts	2.10	2.33	92.35	0.33	8100.88	1.94	2229.11	1.68	15081.68	1.74
CT_Carotid	1.95	2.15	81.13	0.35	7417.23	1.55	1573.34	1.62	10998.34	1.61
CT_Skull	6.26	6.62	248.98	0.87	21763.61	4.04	5049.56	4.21	33952.48	4.14
CT_Wrist	4.40	4.73	192.70	0.57	18220.76	3.59	4349.34	3.76	28902.94	3.80
MR_Liver_T1	1.68	1.82	83.50	0.33	6258.95	1.22	1255.44	1.36	8630.79	1.34
MR_Liver_T2e1	1.58	1.71	63.72	0.26	5769.38	1.20	1160.53	1.14	7892.48	1.11
MR_Ped_Chest	2.10	2.25	102.12	0.36	9014.00	1.57	1591.32	1.56	11168.58	1.54
MR_Sag_Head	1.77	1.89	79.08	0.32	5651.71	1.20	1189.31	1.15	8000.95	1.05
Average	2.73	2.94	117.95	0.42	10274.57	2.04	2299.74	2.06	15578.53	2.04

TABLE XI

RUNNING TIMES (IN SECONDS) FOR THE COMPRESSION OF THE TEST SET 2 (16 BIT-DEPTH CONTENTS) USING JP3D, HEVC AND 3D-MRP

Test Set 2	JP3D		HEVC-Rext		3D-MRP-I3		3D-MRP-I25	
	Encoder	Decoder	Encoder	Decoder	Encoder	Decoder	Encoder	Decoder
CT_Head	5.62	5.70	156.63	0.82	2541.12	3.03	17451.75	3.02
CT_Head_Remb	3.14	3.23	101.05	0.54	1338.20	1.52	9393.00	1.41
CT_Lung_R4	15.52	15.92	430.10	2.05	13785.41	6.94	94992.72	6.89
CT_Lung_R13	14.22	14.64	486.36	2.32	13865.59	7.22	95616.14	7.16
CT_Esophagus	24.64	26.25	876.00	3.12	34168.09	15.10	220148.72	15.07
MR_Brain	6.30	6.43	168.75	0.80	2570.54	3.47	17847.00	3.47
MR_Neuro	9.59	9.55	262.64	1.27	4738.77	4.07	32536.12	3.96
MR_Breast	3.69	3.78	84.64	0.46	1949.70	3.65	15689.96	3.57
Average	10.34	10.69	320.77	1.42	9369.68	5.57	62959.43	5.57

In Table IX, the compression results for the Test Set 2 are presented. For this case only the codecs supporting 16 bit-depth images were used in these experiments. These algorithms include most of the ones used for Test Set 1, and additionally, the Martin Briano implementation of the image-based CALIC (referred to as 2D-CALIC). The 3D-MRP is the only algorithm based on MRP paradigm, because the existing MRP-based algorithms do not support 16 bit-depth images. By observing the results of Table IX, one concludes that 3D-MRP-I25 presents the state-of-the-art results for the compression of volumetric sets of 16 bit-depth medical images, revealing average compression gains close to 0.6 bpp (or 12%) over the HEVC and 2D-CALIC algorithms. When compared to the remaining compression algorithms, the advantage of 3D-MRP is even more noticeable, reaching a gain of almost 1 bpp (or 18%) over the M-CALIC. The less computationally complex version of 3D-MRP, using 3 iterations, presents a slight performance decrease which is inferior to 1%.

Although 3D-CALIC and M-CALIC algorithms are able to exploit inter frame redundancies, these algorithms present the lower average compression results, being less efficient than the 2D-CALIC encoder. This unexpected result can be related to an inefficient implementation of the M- and 3D-CALIC algorithms for the compression of high bit-depth contents.

C. Analysis of the Computational Complexity

As previously explained, the MRP paradigm tends to be significantly complex at the encoder side, while its decoder is computationally simple. Due to this fact, probably 3D-MRP is not the most adequate solution for certain applications, namely when the signal needs to be processed in real-time during its capture. However, this should not be an issue for the case of medical imaging systems. Typically, in medical applications, the whole medical image volume is exported from the equipment after the scanning procedure. Thus, there is no restriction in processing the whole signal after its capture. Moreover, as the medical imaging applications involve the use of dedicated hardware systems, they could be designed to include an efficient hardware implementations of the encoder. Fortunately, due to its forward prediction approach, the MRP-based decoders tend to have a low computational complexity, so that any mid range personal computer is able to decode any volumetric signal rapidly.

The computational complexity of the 3D-MRP encoder is highly dependent on the number of iterations of the optimisation procedure. To demonstrate this statement, the running times of 3D-MRP using 3 and 25 iterations are presented and compared in Tables X and XI. These tests were run in a computer with the Intel Xeon E3-1240 CPU at 3.40GHz and 24GB of RAM, running the Ubuntu Server 16.04 operating system. The most relevant algorithms, with higher compression performance, are also compared, namely the JP3D, HEVC and MRP-Video [28]. Note that the computational complexity of some algorithms, in particular the JPEG-LS, CALIC and MRP, cannot be accurately measured, because they do not encode the full medical image at once. Instead these algorithms are independently called to process each frame. With exception of MRP, these methods present an insignificant computational complexity, using only a few seconds to encode and decode a volumetric medical image.

TABLE XII
MAXIMUM MEMORY USAGE (IN MBYTES) FOR THE COMPRESSION OF THE TEST SET 1 (8 BIT-DEPTH CONTENTS) USING JP3D, HEVC, MRP-VIDEO AND 3D-MRP

Test Set 1	JP3D Encoder	JP3D Decoder	HEVC-Rext Encoder	HEVC-Rext Decoder	MRP-Video [28] Encoder	MRP-Video [28] Decoder	3D-MRP-I3 Encoder	3D-MRP-I3 Decoder	3D-MRP-I25 Encoder	3D-MRP-I25 Decoder
CT_Aperts	288.25	265.37	41.97	13.62	19.77	3.67	228.73	90.26	226.77	90.36
CT_Carotid	271.00	254.18	42.03	13.63	19.67	3.66	204.98	69.70	206.66	69.46
CT_Skull	381.94	337.57	42.21	13.78	19.62	3.67	361.30	182.89	360.02	182.84
CT_Wrist	366.76	324.63	41.99	13.73	19.65	3.73	330.59	163.14	332.70	163.17
MR_Liver_T1	258.93	246.40	42.12	13.72	19.65	3.63	178.76	55.14	179.00	55.03
MR_Liver_T2e1	259.06	246.07	42.11	13.75	19.58	3.72	171.71	53.55	171.86	53.36
MR_Ped_Chest	273.16	256.44	41.93	13.62	19.63	3.70	200.98	70.22	201.15	70.20
MR_Sag_Head	259.03	246.32	42.02	13.70	19.54	3.72	166.13	53.13	166.22	53.09
Average	294.77	272.12	42.05	13.69	19.64	3.69	230.40	92.25	230.55	92.19

TABLE XIII
MAXIMUM MEMORY USAGE (IN MBYTES) FOR THE COMPRESSION OF THE TEST SET 2 (16 BIT-DEPTH CONTENTS) USING JP3D, HEVC AND 3D-MRP

Test Set 2	JP3D Encoder	JP3D Decoder	HEVC-Rext Encoder	HEVC-Rext Decoder	3D-MRP-I3 Encoder	3D-MRP-I3 Decoder	3D-MRP-I25 Encoder	3D-MRP-I25 Decoder
CT_Head	289.73	272.40	74.96	20.91	559.14	103.89	563.01	104.03
CT_Head_Remb	258.91	249.31	74.96	20.86	295.88	59.98	296.18	60.12
CT_Lung_R4	475.14	431.43	216.60	59.97	987.31	261.50	988.47	261.65
CT_Lung_R13	472.19	427.73	217.84	59.88	981.52	257.96	982.82	257.96
CT_Esophagus	826.08	686.00	214.21	59.63	1460.11	609.61	1462.76	609.63
MR_Brain	289.74	275.66	74.93	20.95	765.68	111.70	765.76	111.54
MR_Neuro	361.54	331.70	74.98	21.14	444.07	164.95	445.84	165.08
MR_Breast	303.23	288.06	95.23	27.35	1695.85	126.09	1692.79	126.18
Average	409.57	370.29	130.46	36.33	898.69	212.02	899.70	212.02

As expected, Tables X and XI show that MRP-based algorithms are much more complex than the JP3D and HEVC standards. However, the decoding times of MRP-based methods are reduced, using 2 and 5.5 seconds on average for test sets 1 and 2, respectively. These are faster decoding times than the ones of JP3D that uses 3 and 10.7 seconds on average for test sets 1 and 2, respectively. However, it is important to refer that HEVC presents the fastest decoding times, being inferior to 0.5 and 1.5 seconds for test sets 1 and 2, respectively.

The average running times of 3D-MRP-I25 are about 4.3 hours for test set 1, and 17.5 hours for test set 2. Notwithstanding, these times can be significantly reduced to 38 minutes for test set 1 and 2.6 hours for test set 2, when the number of iterations is reduced to 3. This running time reduction is achieved at the cost of a slight decrease in the compression performance, as discussed in the previous sub-section. When compared with MRP-Video (test set 1), it may be concluded that the faster version of 3D-MRP (using 3 iterations) is about 4 times faster, while still providing a more efficient compression performance (see Table VIII).

Regarding the maximum used memory, achieved results in terms of MBytes are presented in Tables XII and XIII, for test sets 1 and 2, respectively. One may observe that MRP-Video and HEVC present the lowest memory requirements for both test sets. 3D-MRP requires more memory due to the volumetric optimisation, using an average of 230 MB to encode the test set 1 and 900 MB to encode the test set 2. Although these are high values, the JP3D still presents a larger memory usage for the case of the test set 1. The high memory usage of 3D-MRP for the test set 2 can be justified

by the larger dynamic range of these images, which results in larger allocated buffers. At the decoder side, JP3D presents the highest memory usage values for both the test sets.

As future work, sub-optimal methods could be investigated for 3D-MRP algorithm, to reduce its computational complexity. By reducing the number of iterations, it has been shown in this paper that the running times can be significantly improved at the cost of a slight increase of the bitrate. Other algorithms and implementation solutions could be investigated not only to reduce the encoding time but also to minimize the maximum memory used.

VI. CONCLUSION

The 3D-MRP algorithm has been developed for efficient lossless compression of volumetric medical images, using the MRP paradigm at its core, designed for both 8 and 16 bit-depth contents. In addition to 3D-shaped predictors, 3D-MRP uses a volume-based optimisation method, which independently processes groups of 32 frames. An hybrid classification procedure, which enables 2D and 3D block-based classification is presented. Furthermore, several improvements are made to the error probability estimation method of MRP algorithm, which resulted in a better context estimation for higher bit-depth contents.

The experimental results show the high compression efficiency of the 3D-MRP, which achieves average coding gains of 40% and 12% over the HEVC standard, for 8 and 16 bit-depth medical signals, respectively. The superior compression performance of 3D-MRP over the previous presented MRP-based video coding methods demonstrates the importance of

the proposed volumetric coding approach over the traditional frame-based coding approach. In summary, the presented research develops an improved coding algorithm based on minimum rate predictors which achieves state-of-the-art results for the compression of volumetric medical data with higher bit-depth contents.

REFERENCES

[1] O. S. Pianykh, "Digital imaging and communications in medicine," in *A Practical Introduction and Survival Guide*, 1st ed. Berlin, Germany: Springer-Verlag, 2008. [Online]. Available: http://www.springer.com/gp/book/9783642108495

[2] *Information Technology—Digital Compression and Coding of Continuous-Tone Still Images*, document ISO/IEC 10918-1, ITU-T Rec. T.81, 1992.

[3] W. Pennebaker and J. Mitchel, *JPEG: Still Image Data Compression Standard*, 1st ed. Norwell, MA, USA: Kluwer, 1992.

[4] *Information Technology—Lossless and Near-Lossless Compression of Continuous-Tone Still Images: Baseline*, document ISO/IEC 14495-1, ITU-T Rec. T.87, 1998.

[5] M. J. Weinberger, G. Seroussi, and G. Sapiro, "The LOCO-I lossless image compression algorithm: Principles and standardization into JPEG-LS," *IEEE Trans. Image Process.*, vol. 9, no. 8, pp. 1309–1324, Aug. 2000.

[6] *Information Technology—JPEG 2000 Image Coding System: Core Coding System*, document ISO IEC 15444-1, ITU-T Rec. T.800, 2002.

[7] D. S. Taubman and M. Marcelin, *JPEG2000: Image Compression Fundamentals, Standards and Practice*, 2nd ed. Norwell, MA, USA: Kluwer, 2001.

[8] *Generic Coding of Moving Pictures and Associated Audio Information— Part 2: Video*, document ITU-T Recommendation H.262, ISO/IEC 13818-2 (MPEG-2), ITU-T and ISO/IEC JTC1, Jul. 1995.

[9] *Advanced Video Coding for Generic Audiovisual Services*, document ITU-T Recommendation H.264, ISO/IEC 14496-10 (MPEG-4 AVC), ITU-T and ISO/IEC JTC1, May 2003.

[10] T. Wiegand, G. J. Sullivan, G. Bjøntegaard, and A. Luthra, "Overview of the H.264/AVC video coding standard," *IEEE Trans. Circuits Syst. Video Technol.*, vol. 13, no. 7, pp. 560–576, Jul. 2003.

[11] *Information Technology—JPEG 2000 Image Coding System: Extensions*, document ISO/IEC 15444-2, ITU-T Rec. T.801, 2002.

[12] *Information Technology—JPEG 2000 Image Coding System: Extensions for Three-Dimensional Data*, document ISO/IEC 15444-10, ITU-T Rec. T.809, 2011.

[13] *High Efficiency Video Coding*, document ITU-T Recommendation H.265 and ISO/IEC 23008-2, ITU-T and ISO/IEC JTC1, Apr. 2013.

[14] G. J. Sullivan, J.-R. Ohm, W.-J. Han, and T. Wiegand, "Overview of the High Efficiency Video Coding (HEVC) standard," *IEEE Trans. Circuits Syst. Video Technol.*, vol. 22, no. 12, pp. 1649–1668, Dec. 2012.

[15] T. Bruylants, A. Munteanu, and P. Schelkens, "Wavelet based volumetric medical image compression," *Signal Process. Image Commun.*, vol. 31, pp. 112–133, Feb. 2015.

[16] V. Sanchez, R. Abugharbieh, and P. Nasiopoulos, "3-D scalable medical image compression with optimized volume of interest coding," *IEEE Trans. Med. Imag.*, vol. 29, no. 10, pp. 1808–1820, Oct. 2010.

[17] V. Sanchez, R. Abugharbieh, and P. Nasiopoulos, "Symmetry-based scalable lossless compression of 3D medical image data," *IEEE Trans. Med. Imag.*, vol. 28, no. 7, pp. 1062–1072, Jul. 2009.

[18] Z. Xu *et al.*, "Diagnostically lossless coding of X-ray angiography images based on background suppression," *Comput. Electr. Eng.*, vol. 53, pp. 319–332, Sep. 2016.

[19] X. Wu and N. Memon, "Context-based, adaptive, lossless image coding," *IEEE Trans. Commun.*, vol. 45, no. 4, pp. 437–444, Apr. 1997.

[20] X. Li and M. T. Orchard, "Edge-directed prediction for lossless compression of natural images," *IEEE Trans. Image Process.*, vol. 10, no. 6, pp. 813–817, Jun. 2001.

[21] I. Matsuda, H. Mori, and S. Itoh, "Lossless coding of still images using minimum-rate predictors," in *Proc. Int. Conf. Image Process.*, vol. 1. 2000, pp. 132–135.

[22] I. Matsuda, Y. Umezu, N. Ozaki, J. Maeda, and S. Itoh, "A lossless coding scheme using adaptive predictors and arithmetic code optimized for each image," *Syst. Comput. Jpn.*, vol. 38, no. 4, pp. 1–11, 2007.

[23] E. Magli, G. Olmo, and E. Quacchio, "Optimized onboard lossless and near-lossless compression of hyperspectral data using CALIC," *IEEE Geosci. Remote Sens. Lett.*, vol. 1, no. 1, pp. 21–25, Jan. 2004.

[24] X. Wu and N. Memon, "Context-based lossless interband compression-extending CALIC," *IEEE Trans. Image Process.*, vol. 9, no. 6, pp. 994–1001, Jun. 2000.

[25] I. Matsuda, T. Shiodera, and S. Itoh, "Lossless video coding using variable block-size MC and 3D prediction optimized for each frame," in *Proc. 12th Eur. Signal Process. Conf.*, Sep. 2004, pp. 1967–1970.

[26] I. Matsuda, T. Shiodera, H. Maeda, and S. Itoh, "Lossless video coding using bi-directional 3D prediction optimized for each frame," in *Proc. Eur. Conf. Circuit Theory Design*, vol. 2. Aug. 2005, pp. II-71–II-74.

[27] H. Maeda, A. Minezawa, I. Matsuda, and S. Itoh, "Lossless video coding using multi-frame MC and 3D bi-prediction optimized for each frame," in *Proc. 14th Eur. Signal Process. Conf.*, Sep. 2006, pp. 1–5.

[28] J. M. Santos, A. F. R. Guarda, N. M. M. Rodrigues, and S. M. M. Faria, "Contributions to lossless coding of medical images using minimum rate predictors," in *Proc. IEEE Int. Conf. Image Process.*, Sep. 2015, pp. 2935–2939.

[29] *MRP Codec Version 0.5*, accessed on Feb. 1, 2015. [Online]. Available: http://itohws03.ee.noda.sut.ac.jp/ matsuda/mrp/mrp-05.tar.gz

[30] I. Matsuda, N. Shirai, and S. Itoh, "Lossless coding using predictors and arithmetic code optimized for each image," in *Proc. 8th Int. Workshop Vis. Content Process. Represent. (VLBV)*, Berlin, Germany, Sep. 2003, pp. 199–207.

[31] *Cipr Sequences 01*, accessed on Apr. 20, 2017. [Online]. Available: http://www.cipr.rpi.edu/resource/sequences/sequence01.html

[32] *The Stanford Volume Data Archive*, accessed on Apr. 20, 2017. [Online]. Available: https://graphics.stanford.edu/data/voldata/

[33] *The Cancer Imaging Archive*, accessed on Apr. 20, 2017. [Online]. Available: http://www.cancerimagingarchive.net/

[34] K. Clark *et al.*, "The cancer imaging archive (TCIA): Maintaining and operating a public information repository," *J. Digit. Imag.*, vol. 26, no. 6, pp. 1045–1057, 2013.

[35] (2015). K. Smith *et al. Data From REMBRANDT The Cancer Imaging Archive*. [Online]. Available: http://dx.doi.org/10.7937/K9/TCIA.2015.588OZUZB

[36] (2015). O. Grove. *Data From: Quantitative Computed Tomographic Descriptors Associate Tumor Shape Complexity and Intratumor Heterogeneity With Prognosis in Lung Adenocarcinoma The Cancer Imaging Archive*. [Online]. Available: http://doi.org/10.7937/K9/TCIA.2015.A6V7JIWX

[37] O. Grove *et al.*, "Quantitative computed tomographic descriptors associate tumor shape complexity and intratumor heterogeneity with prognosis in lung adenocarcinoma," *PLoS ONE*, vol. 10, no. 3, pp. 1–14, Mar. 2015.

[38] (2016). K. Smith *et al. Radiology Data From the Cancer Genome Atlas Esophageal Carcinoma [TCGA-ESCA] Collection The Cancer Imaging Archive*. [Online]. Available: http://doi.org/10.7937/K9/TCIA.2016.VPTNRGFY

[39] (2015). K. Smith *et al. Data From RIDER_NEURO_MRI The Cancer Imaging Archive*. [Online]. Available: http://dx.doi.org/10.7937/K9/TCIA.2015.VOSN3HN1

[40] (2015). Meyer. *Data From RIDER_Breast_MRI The Cancer Imaging Archive*. [Online]. Available: http://doi.org/10.7937/K9/TCIA.2015.H1SXNUXL

[41] *Hp Labs Loco-I/JPEG-LS Home Page*, accessed on Apr. 20, 2017. [Online]. Available: http://www.labs.hp.com/research/info_theory/loco/

[42] *An Open-Source JPEG 2000 Codec Written in C*, accessed on Apr. 20, 2017. [Online]. Available: http://www.openjpeg.org/

[43] *Calic Implementation*, accessed on Apr. 20, 2017. [Online]. Available: http://www.ece.mcmaster.ca/ xwu/calicexe/

[44] *3D-Calic Implementation*, accessed on Apr. 20, 2017. [Online]. Available: https://prezi.com/j2ichhip4ls7/calic-implementation/